ChemComm

Accepted Manuscript

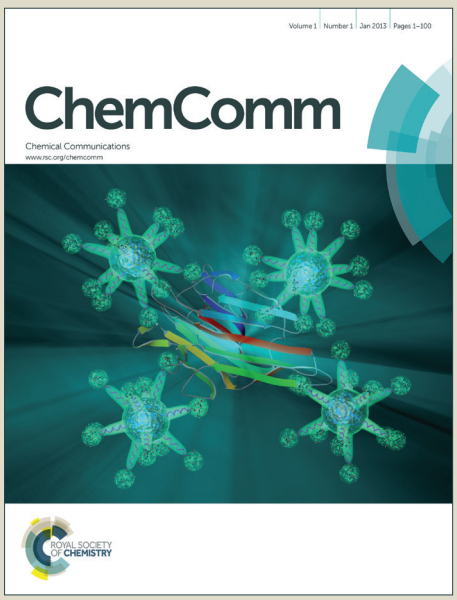

ROYAL SOCIETY OF CHEMISTRY

www.rsc.org/chemcomm

Promising two-photon probes for in-vivo detection of β amyloid deposits†

N. Arul Murugan,*[,a] Robert Zaleśny,[a,b] Jacob Kongsted,[c] Agneta Nordberg[d] and Hans Ågren[a]

Received Xth XXXXXXXXXX 20XX, Accepted Xth XXXXXXXXX 20XX
First published on the web Xth XXXXXXXXXX 200X
DOI: 10.1039/b000000x

Based on electronic structure calculations we propose that particular small-sized organic molecules - donor-acceptor substituted phenyl polymethines - can be used as two-photon diagnostic probes for non-invasive imaging of amyloid oligomers and fibrils which are often referred to as the "early signature" of Alzheimer's disease.

The changes in the secondary structure of peptides, aggregation and fibril formation have been proposed to be the molecular processes that are associated with the initial stages of a number of so-called "protein conformational diseases" such as Alzheimer's, Parkinsons, Wilson's diseases and many more.[1] Although it is more than 100 years now after the detection of the fibril deposits in the brain of people succumbed to Alzheimer's disease, it still remains a major challenge for the scientific community working on the diagnosis of these diseases to develop effective and bio-friendly diagnostic agents for in-vivo imaging of the oligomers and fibrils of amyloid and Tau proteins. Today Thioflavin T and Congo red-based radio-nucleotide labeled diagnostic agents are commonly used for detecting fibrils using PET and SPECT imaging technologies.[2,3] However, there is an ongoing quest for new and more efficient alternatives, which also can lower cost and health risk associated with the radiation and hazardous nature of the now used imaging agents.[4] Optical imaging-based approaches are associated with lower health risk, but suffer often from aggravating factors like probe auto-fluorescence or limited capability for tissue penetration. Although two-photon microscopy-based imaging[5] possesses a number of advantages over commonly used fluorescence imaging, such as increased tissue permeability,[6] possibility for the usage of less harmful IR radiation, and increased temporal and spatial resolution, to our knowledge, applications for fibril imaging lack so far. Such two-photon microscopy-based imaging would involve the administration of diagnostic agents that have strong binding affinity towards fibrils and that possess large two-photon absorption (TPA) cross sections. In addition, similar to other drugs administered to the brain, they should be able to pass through the blood-brain barrier (BBB) which adds additional requirements for the diagnostic agents to be used for in-vivo imaging of fibrils in brains, like low molecular weight and increased lipophilicity. Unfortunately, there are only a few fluorescent probes and PET/SPECT tracers such as the Pittsburgh-B (PIB) compound and a naphthalene analog of PIB, bis-styrylbenzene derivative, a dimethylamino substituted GFP-type chromophore (DMC),[7–9] for the in-vivo imaging of fibrils that fulfill these requirements. Moreover, the two-photon absorption cross section values measured for these compounds are not very promising. For example, the TPA value associated with DMC is only 32 GM.[8] It is clearly evident that there is a need to develop novel TPA diagnostic agents for fibril imaging. In this context it should also be highlighted that amyloids exhibit strong nonlinear optical absorption, which is not present in native non-fibrillized protein.[10] However, the two photon absorption band maximum in this case is located at 550 nm.

A potential route to identify effective two-photon probes for fibril imaging is to explore the two-photon properties of diagnostic agents that already have shown some success in fluorescence-based imaging of fibrils. There are many such agents based on Thioflavin T, distyryl benzene-like (i.e. Congo Red), polypyrrole-like[11] and donor-π-acceptor type structural motifs. Due to the established correlation between the donor-π-acceptor structural motif and properties like polarizability, first hyperpolarizability and two-photon absorption cross sections,[12–14] we study in this article donor-π-acceptor substituted phenyl polymethine-based molecules for their potential use for the two-photon imaging of fibrils in brains. In fact, the molecules investigated herein have been experimentally reported to have nanomolar binding affinity to-

† Electronic Supplementary Information (ESI) available: [Details of electronic structure calculations]. See DOI: 10.1039/b000000x/

[a] *Division of Theoretical Chemistry and Biology, School of Biotechnology, Royal Institute of Technology, SE-10691 Stockholm, Sweden. E-mail: murugan@theochem.kth.se (N.A.M).*
[b] *Institute of Physical and Theoretical Chemistry, Wrocław University of Technology, Wyb. Wyspiańskiego 27, PL-50370, Wrocław, Poland.*
[c] *Department of Physics, Chemistry and Pharmacy, University of Southern Denmark, Campusvej 55, DK-5230 Odense M, Denmark*
[d] *Karolinska Institute, Department of Clinical Neuroscience, Division of Molecular Neuropharmacology, Huddinge University Hospital, B 84, S-141 86 Stockholm, Sweden.*

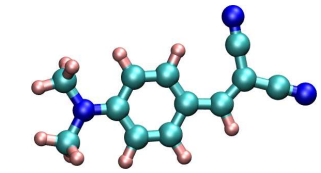

(a) NIRF-0

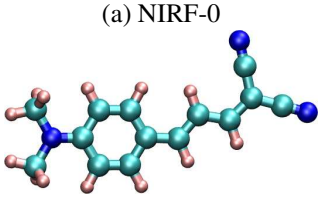

(b) NIRF-1

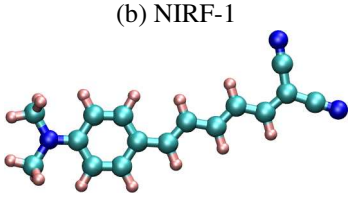

(c) NIRF-2

Fig. 1 The molecular probes studied in this work. Coloring scheme: cyan (carbon), blue (nitrogen), grey (hydrogen)

Table 1 Vertical excitation energies (TDDFT/CAM-B3LYP/TZVP level of theory) and experimental absorption band maxima (in nm) for the three NIRF compounds. The oscillator strength is given in parenthesis. Solvent effects are included using the PCM method.

Probe ⇒ Methods ⇓	NIRF-0	NIRF-1	NIRF-2
Calc.	378 (1.12)	438 (1.60)	492 (2.08)
Expt.	433	489	519

wards fibrils and have been verified to pass through the blood-brain barrier,[15] thus already fulfilling two of the primary requests. The molecular structures of these near-infrared fluorescent probes (hereafter referred to as NIRF-*n*, *n*=0,1,2) studied herein are shown in Figure 1. Even though they have been reported to be successful diagnostic agents for fluorescence imaging,[15] we thus aim at characterizing the potential of these molecules as two-photon probes for fibril imaging. The rationale behind this motivation is that currently there are no available reports of effective two-photon probes for fibril imaging that have the capability to pass through the BBB. Additionally, we aim to set out possible structure-property relationships for future design of improved diagnostic probes.

One of the possible routes to tune two-photon absorption properties is through modification of the bond-length alternation (BLA), which is defined as the difference between the average single and double bonds along the conjugation pathway.[14] The BLA parameter has been shown to correlate with many properties like, for instance, the polarizability, the first and second hyperpolarizability, the two-photon absorption cross section, and the solvatochromic shift or NMR spin-spin coupling constants.[12–14,16] The computed values of the BLA for all three NIRFs (see ESI for more information) are 0.04, 0.07 and 0.10 Å , respectively. These numbers suggest that the increase in spacer group length leads to BLA increase. The positive sign of the BLA further suggests that the ground state electronic structure remains neutral-like, independent of the increase in the spacer group length.

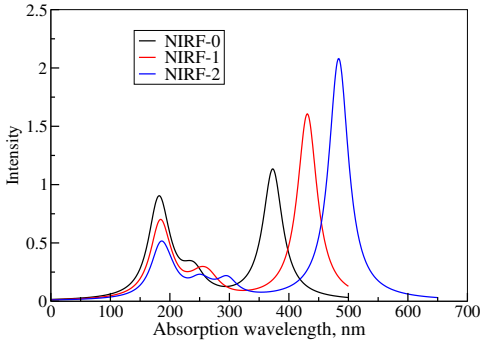

Fig. 2 Absorption spectra for the three NIRF compounds simulated at the CAM-B3LYP/TZVP level of theory. Solvent effects are included using the PCM method.

Figure 2 shows the computed UV-visible absorption spectra for the NIRFs compounds. Details of all electronic structure calculations are presented in ESI. In all three cases, it exhibits two intense bands - one appearing in the visible region and the other appearing in the UV region of the spectrum. Interestingly, the position of the second intense band remains the same for all systems. However, the first band exhibits a red-shift upon elongation of the conjugation path and the corresponding absorption intensity increases. The computed wavelength corresponding to vertical electronic transition for the three NIRF systems are compared to experimental values of the absorption band maxima in Table 1. Even though the computed values are blue shifted when compared to experimental values, the increase in excitation energy with spacer group length is reproduced satisfactorily. Note that effects of nuclear motion, which may contribute to the observed discrepancies, are not included in our treatment. The computed two-photon absorption cross sections corresponding to the few lowest excited states are presented in Table 2. The results are shown for both gas phase environment and in dichloromethane solvent. There are interesting features which are worth highlighting: (i) The TPA cross section values for the NIRF probes for the first band in dichloromethane solvent are two times larger than in the gas phase which reveals a substantial solvent effect on the studied property. This suggests that NIRF probes exhibit two photon solvatochromism like DANS and Reichardt's dye. (ii) The two-photon absorption cross section increases from 68 to 503 GM (33 to 239 GM in the gas phase)

Table 2 Two-photon absorption cross section (in GM) calculated for NIRF0-NIRF2 in dichloromethane solvent and *in vacuo* (values are given in parenthesis). Also included is the excitation wavelength (in nm) together with a reference for the relevant excited state (S_i). Note that for NIRF-0 state number 4 and 5 interchange upon introducing the effect of the solvent.

NIRF-0		NIRF-1		NIRF-2	
S_1, 756	68 (33)	S_1, 876	202 (101)	S_1, 984	503 (239)
S_5, 464	773 (279, S_4)	S_3, 532	2339 (766)	S_2, 599	6141 (1560)

going from NIRF-0 to NIRF-2 in what corresponds to a 7-fold increase upon spacer elongation, (iii) Interestingly, the first intense two-photon band in the case of NIRF-1 and NIRF-2 appears to have absorption in the IR region of the spectrum which brings the possibility to probe a deeper region. It is also notable that the second band in NIRF-2 has 6000 GM which is very large considering the size of the molecule, however, the absorption wavelength remains in the visible region (i.e. ≈600 nm).

In order to gain insight into the various electronic structure parameters and their relation with the two-photon transition probability (δ), a two-state model (2SM) analysis has been performed in which the two-photon transition probability is expressed as

$$\delta^{2SM} = \frac{16}{15}\frac{|\mu^{0i}|^2|\Delta\mu|^2}{\omega^2}(1+2\cos^2\theta_{\Delta\mu}^{\mu^{0i}}) \quad (1)$$

where μ^{0i} and $\Delta\mu$ refer to the transition dipole from the ground to the i'th excited state and the difference between the excited and ground state dipole moments, respectively. The $\theta_{\Delta\mu}^{\mu^{0i}}$ refers to the angle between these two vectors while ω refers to the excitation energy. The values of these parameters involved in the two-state model are presented in Table 3. Considering

Table 3 Two-state model analysis parameters. All numbers are reported in au and are based on calculations for NIRF0-2 in isolation. The numbers in parentheses refer to the response theory values determined using all eigenstates.

State	μ_{0i}	$\Delta\mu$	$\theta_{\Delta_\mu}^{\mu_{0i}}$	δ^{2SM}
		NIRF-0		
1	1.415	3.280	179.9	3903 (4317)
4	0.683	0.825	130.3	15 (13222)
		NIRF-1		
1	1.963	4.274	5.3	16196 (18124)
3	0.968	0.917	120.6	40 (49622)
		NIRF-2		
1	2.568	5.201	6.0	49790 (56565)
2	1.483	1.212	129.4	240 (130475)

the first intense TPA band (i=1), the agreement between the δ^{2SM} value and the response theory value is fairly good. As it is seen, all three parameters such as excitation energy, dipole moment difference and transition dipole moment and the almost parallel (or antiparallel) alignment of $\Delta\mu$ and μ_{01} are contributing to the increase in δ when going from NIRF-0 to NIRF-1. Even though the increase in δ values is still captured by the two-state model for the second intense TPA band (i=4 for NIRF-0, i=3 for NIRF-1 and i=2 for NIRF-2), the quantitative agreement with the values computed from response theory is far from satisfactory. In fact, this indicates that other optical channels involving intermediate states contribute dominantly to the TPA process which is not accounted in the simplistic two-state model. Thus, a few state model[17,18] has been used to shed light on the TPA mechanism. As can be seen the δ^{3SM} (three-state model) values are in good agreement with the numbers predicted from response theory (cf. Table 4). In all three cases, the optical channel involving the lowest excited state, as the intermediate state, dominantly contributes to the δ values. As can be seen the 2SM and 3SM explain the enhancement in two photon transition probability with increase in spacer group length for the first and second intense TPA band. However, these involve 3 and 4 parameters, respectively, and it is convenient to find a single parameter correlation with δ (and two-photon absorption cross section) values to establish novel structure-property relationships to be used for design of efficient two photon materials.

Table 4 Three-state model analysis for the second intense TPA band. The symbols are defined in ESI. The index "full" refers to the response theory value determined using all eigenstates. The index f and i refer to final and intermediate states respectively.

System	f	i	δ_{ii}	δ_{ff}	δ_{if}	$\delta^{0\to f}_{(3SM)}$	$\delta^{0\to f}_{(full)}$
NIRF-0	4	1	12907	877	2654	19093	12600
NIRF-1	3	1	46820	2272	9672	68436	44600
NIRF-2	2	1	118548	7599	29826	185799	111000

With this focus, in what follows we will explore the potential of a newly proposed intramolecular charge transfer descriptor[19] with an eye towards its application to design novel TPA-active materials:

$$\Delta r = \frac{\sum_{ia} K_{ia}^2 |\langle\phi_a(r)|r|\phi_a(r)\rangle - \langle\phi_i(r)|r|\phi_i(r)\rangle|}{\sum_{ia} K_{ia}^2} \quad (2)$$

where K is a vector defined as the sum of the excitation and de-excitation parts of the linear response vector.[20] The Δr index, is based on the orbital centroids computed for the molecular orbitals (referred to as i and a) involved in the excitation and is a measure for the average hole-electron distance upon excitation. It is related to the dipole moment difference between the excited state and the ground state. On the

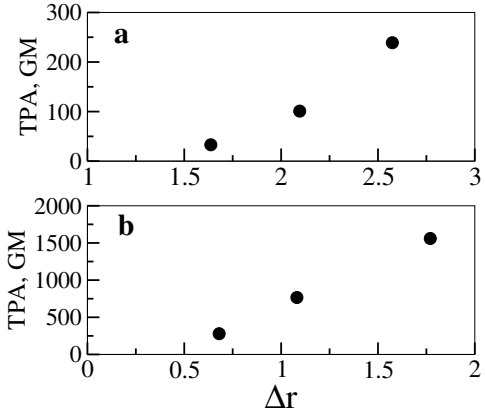

Fig. 3 The relationship between the charge transfer descriptor, Δr and TPA cross sections for the first (top) and for the second (bottom) intense band

other hand, the two-level model predicts the following dependence between the two-photon absorption cross section and the dipole moment difference: $\sigma^{2PA} \propto (\mu^{0i})^2(\Delta\mu)^2$. One may thus anticipate a relationship between σ^{2PA} and Δr. In Fig. 3 we plot the values for the charge-transfer descriptor against the TPA cross section values (corresponding to the first two low-energy but intense TPA bands) for the three NIRF systems. As can be seen from the figure the average hole-electron distance upon excitation correlates very well with the TPA cross section values corresponding to both bands. The increase in Δr suggests an increased charge transfer distance upon the electronic excitation and should so lead to an increased TPA cross section value and which, in fact, is seen in these figures. Moreover, almost a linear relationship is observed between the Δr and TPA cross section values suggesting that this descriptor can be used as a "two photon diagnostic" of the donor-acceptor substituted polymethine molecules studied herein. Interestingly, unlike the few-state models it works for both intense TPA bands.

Motivated by some salient characteristics of two-photon excited (TPA) fluorescence spectroscopy, like increased tissue penetration, confocality and lowered autofluorescence, we have in this work studied a class of molecular TPA probes for their use in Alzheimer fibril detection. By studying diagnostic agents that have already shown some success in fluorescence-based imaging of fibrils the prerequisites of blood-brain barrier penetration and fibril binding are already fulfilled. With full *ab initio* response theory calculations used simultaneously with a few-state model and charge transfer descriptor calculations, we arrive at the conclusion that these NIRF probes provide promisingly large cross sections for two-photon probing, in particular those containing large spacer groups. We foresee further work in this area exploiting *ab initio* modeling and structure-property relation for two-photon absorption combined with biomedical data and measurements for their selectivity, binding and biocompatibility.

Acknowledgments: This work was supported by the Swedish Infrastructure Committee (SNIC) for the project "Multi-physics Modeling of Molecular Materials", SNIC025/12-38. The work was also financed by the Polish Ministry of Science and Higher Education within "Iuventus Plus" programme (Grant No. 0628/IP3/2011/71). R.Z. is a Wenner-Gren Foundations scholar. J.K. thanks the Danish Center for Scientific Computing (DCSC), The Danish Councils for Independent Research (The Sapere Aude programme), the Lundbeck Foundation and the Villum foundation for financial support.

References

1 C. Soto, *FEBS Letters*, 2001, **498**, 204 – 207.
2 W. E. Klunk, H. Engler, A. Nordberg, Y. Wang, G. Blomqvist, D. P. Holt, M. Bergström, I. Savitcheva, G.-F. Huang, S. Estrada, B. Ausén, M. L. Debnath, J. Barletta, J. C. Price, J. Sandell, B. J. Lopresti, A. Wall, P. Koivisto, G. Antoni, C. A. Mathis and B. Långström, *Annals of Neurology*, 2004, **55**, 306–319.
3 C. A. Mathis, B. J. Bacskai, S. T. Kajdasz, M. E. McLellan, M. P. Frosch, B. T. Hyman, D. P. Holt, Y. Wang, G.-F. Huang and M. L. Debnath, *Bioorganic & medicinal chemistry letters*, 2002, **12**, 295–298.
4 A. Nordberg, J. O. Rinne, A. Kadir and B. Långström, *Nature Reviews Neurology*, 2010, **6**, 78–87.
5 W. R. Zipfel, R. M. Williams and W. W. Webb, *Nat Biotech*, 2003, **21**, 1369–1377.
6 F. Helmchen and W. Denk, *Nat Meth*, 2005, **2**, 932–940.
7 C. H. Heo, K. H. Kim, H. J. Kim, S. H. Baik, H. Song, Y. S. Kim, J. Lee, I. Mook-Jung and H. M. Kim, *Chemical Communications*, 2013, **49**, 1303–1305.
8 T. B. Clark, M. Ziółkowski, G. C. Schatz and T. Goodson III, *The Journal of Physical Chemistry B*, 2014, **118**, 2351–2359.
9 W. E. Klunk, H. Engler, A. Nordberg, Y. Wang, G. Blomqvist, D. P. Holt, M. Bergström, I. Savitcheva, G.-F. Huang, S. Estrada *et al.*, *Annals of neurology*, 2004, **55**, 306–319.
10 P. Hanczyc, M. Samoc and B. Norden, *Nature Photonics*, 2013, **7**, 969–972.
11 K. P. R. Nilsson, A. Åslund, I. Berg, S. Nyström, P. Konradsson, A. Herland, O. Inganäs, F. Stabo-Eeg, M. Lindgren, G. T. Westermark *et al.*, *ACS chemical biology*, 2007, **2**, 553–560.
12 G. Bourhill, J.-L. Bredas, L.-T. Cheng, S. R. Marder, F. Meyers, J. W. Perry and B. G. Tiemann, *J. Am. Chem. Soc.*, 1994, **116**, 2619–2620.
13 M. Albota, D. Beljonne, J.-L. Brédas, J. E. Ehrlich, J.-Y. Fu, A. A. Heikal, S. E. Hess, T. Kogej, M. D. Levin, S. R. Marder, D. McCord-Maughon, J. W. Perry, H. Röckel, M. Rumi, G. Subramaniam, W. W. Webb, X.-L. Wu and C. Xu, *Science*, 1998, **281**, 1653–1656.
14 N. A. Murugan, J. Kongsted, Z. Rinkevicius and H. Ågren, *Proc. Natl. Acad. Sci. (USA)*, 2010, **107**, 16453–16458.
15 M. Cui, M. Ono, H. Watanabe, H. Kimura, B. Liu and H. Saji, *J. Am. Chem. Soc.*, 2014, **136**, 3388–3394.
16 F. Meyers, S. Marder, B. Pierce and J. Bredas, *Journal of the American Chemical Society*, 1994, **116**, 10703–10714.
17 P. Cronstrand, Y. Luo and H. Ågren, *Chemical physics letters*, 2002, **352**, 262–269.
18 M. M. Alam, M. Chattopadhyaya and S. Chakrabarti, *Phys. Chem. Chem. Phys.*, 2012, **14**, 1156–1165.
19 C. A. Guido, P. Cortona, B. Mennucci and C. Adamo, *Journal of Chemical Theory and Computation*, 2013, **9**, 3118–3126.
20 M. J. G. Peach, P. Benfield, T. Helgaker and D. J. Tozer, *J. Chem. Phys.*, 2008, **128**, 044118.